

EFFECTS OF LATERAL PLATE DIMENSIONS ON ACOUSTIC EMISSION SIGNALS FROM DIPOLE SOURCES

M. A. HAMSTAD*, A. O'GALLAGHER and J. GARY

National Institute of Standards and Technology, Boulder, CO 80305

* Department of Engineering, University of Denver, Denver, CO 80108

ABSTRACT

With a validated three-dimensional finite element code, the out-of-plane displacements corresponding to model sources of acoustic emission (AE) were calculated in aluminum plate samples of two different lateral dimensions. Both samples were 4.7 mm thick. The lateral dimensions were 480 mm by 25.4 mm, which represented a laboratory-size coupon, versus 1000 mm by 1000 mm, which represented a larger field-size sample. The displacement signals were calculated for positions of the receiver on the top plate surface at several different distances (in the far-field) from the source's epicenter. The signals were predicted for the same propagation distances of source-to-receiver in both the large and small samples. Models of both point-like sensors as well as sensors with a large aperture were used. The signals were filtered with either a 40-kHz high-pass filter or a 100-to-300-kHz bandpass filter. The AE sources were modeled as either a point single dipole (both in-plane and out-of-plane) or a point multi-dipole located at different depths within the plate thickness. Analysis of the simulated AE signals shows that the superposition of edge reflections on the arrivals of the direct signal significantly distorts and amplifies AE signals in the laboratory-size coupon relative to a larger field-sized sample. This results in significantly larger AE signal features such as amplitude, duration, and energy in the laboratory-sized sample. Edge reflections also distort the frequency spectrum of signals in the small sample.

1. INTRODUCTION

Since acoustic emission (AE) technology is widely used in both laboratory settings and field testing of large structures, a broad range of dimensions of test samples is encountered. Thus, some sample dimensions are conveniently described in millimeters and others in meters. A natural question arises; what effects do the sample dimensions have on the measured AE signals? In particular, how do these changes in signal affect the identification of the source of the detected AE? Further, what are the effects of specimen size on the detectability of AE and the determination of the significance of detected AE? The research described herein used a recently developed and validated dynamic-finite-element modeling method for wave propagation (Hamstad et al., 1999; Prosser et al., 1999) to examine the effects on predicted AE signals of varying the lateral dimensions of plate specimens. For the two different specimen dimensions considered, the same sensor positions relative to the source (i.e., propagation distances) were modeled. Due to the ability to include reflections from all sample boundaries (including the edges of the plate), the finite-element method can fully model cases that analytical AE modeling approaches have been unable to address.

Contribution of the U.S. National Institute of Standards and Technology; not subject to copyright in the US.

An earlier study (Gorman, 1998) used experimental techniques to study the effects of lateral plate dimensions. However, the experimental source was an out-of-plane surface-applied pencil-lead break, which does not accurately represent an internal AE crack source. The current study modeled *buried dipole* point sources, which more closely represent real AE sources than lead-break *surface monopole* sources. Further, the previous study did not compare the AE signals at exactly the same distances from the source to the sensor in the small and large plates. Thus, quantitative comparisons with parameters such as peak signal amplitude were not possible. The current study does allow such comparisons. The current study also examines specimen dimension effects on frequency spectra. Both wideband point-type sensors as well as sensors of larger aperture with narrowband sensitivity are modeled.

2. FINITE ELEMENT AND SOURCE CONDITIONS

An extensive database was created by calculating AE signals for three different types of buried sources and several different source depths in the plate samples. In particular, the buried sources were (i) an in-plane single dipole aligned along the direction of propagation to the sensors; (ii) an out-of-plane single dipole; and (iii) a multi-dipole with three dipoles that represent initiation of a microcrack source (Scruby, 1985). For the latter source, the strongest dipole was again in-plane and aligned along the direction of propagation to the sensors. The dipole forces (body forces) were all 1 N except for the two smaller dipoles in the microcrack case, which were 0.52 N (based on the elastic constants of aluminum). Each dipole was made up of a "central" cell having no body force along with single cells on each side of the "central" cell having the body forces. This approach follows that used in a buried-source finite-element validation study (Hamstad et al., 1999). The source body forces had a "cosine bell" temporal dependence with a rise time of 1.5 μs . All the calculations were based on a uniform three-dimensional cell size of 0.313 mm (except as noted below). The material constants for the 4.7-mm-thick aluminum plate samples were: a bulk longitudinal velocity of 6320 m/s, a shear velocity of 3100 m/s, and a density of 2700 kg/m³. The modeled sensor outputs were the out-of-plane top-surface displacement from a single nodal point for point-type sensors, and from the average of all the nodal points in a circle of 13-mm diameter in the case of a finite aperture sensor. The parameters for the finite-element code were selected in accordance with the conditions previously (Hamstad et al., 1999) determined to be necessary to model point sources with a particular rise time. In one case, convergence was checked by proving the modeled AE signals did not change for a calculation with a cell size decreased by 20 %. The conditions necessary for convergence (Hamstad et al., 1999) resulted in a time step of 44.62 ns for the computations, which were carried out for a total of 200 μs after the start of the operation of the dipole sources. For all the waveform figures in this paper, the zero time is the start of operation of the dipole source.

3. LATERAL PLATE GEOMETRY AND SOURCE/SENSOR LOCATIONS

The choice of geometry for the small coupon specimen was taken from a previous experimental study (McBride and Hong, 1992), in which a sample 480 mm by 25.4 mm was used to study the AE generated from fatigue crack growth in specimens of 7000-series aluminum alloys 4.7 mm thick. Lateral dimensions of 1000 mm by 1000 mm (4.7 mm thick) were selected

to represent a field-test configuration that does not have nearby sample edges. These lateral dimensions were sufficiently large such that reflections from the sample edges did not superimpose on directly arriving signals. A total of seven point-type sensor positions were selected. Two coincided with the sensor positions used in the referenced original experimental study. For the finite-element simulation, these two positions were modeled to obtain displacements representing both point-type and finite-aperture sensors. Figure 1 is a drawing of the small specimen superimposed on the large sample, identifying the various sensor positions along with the source position. The locations for the finite-aperture sensors used in the referenced crack-propagation study are at locations 2 and 5 (see Fig. 1) at 120 mm and 60 mm from the plane that contained the source. The source position (below sensor 4) is located in the same cross-sectional plane, in which the crack was propagated in the referenced experimental study. For most of the finite element (FEM) cases, the source was located halfway across the width of the small sample (see Fig. 1). A few computations were made with the source in the same plane, but not symmetrically located with respect to the long sides of the small sample.

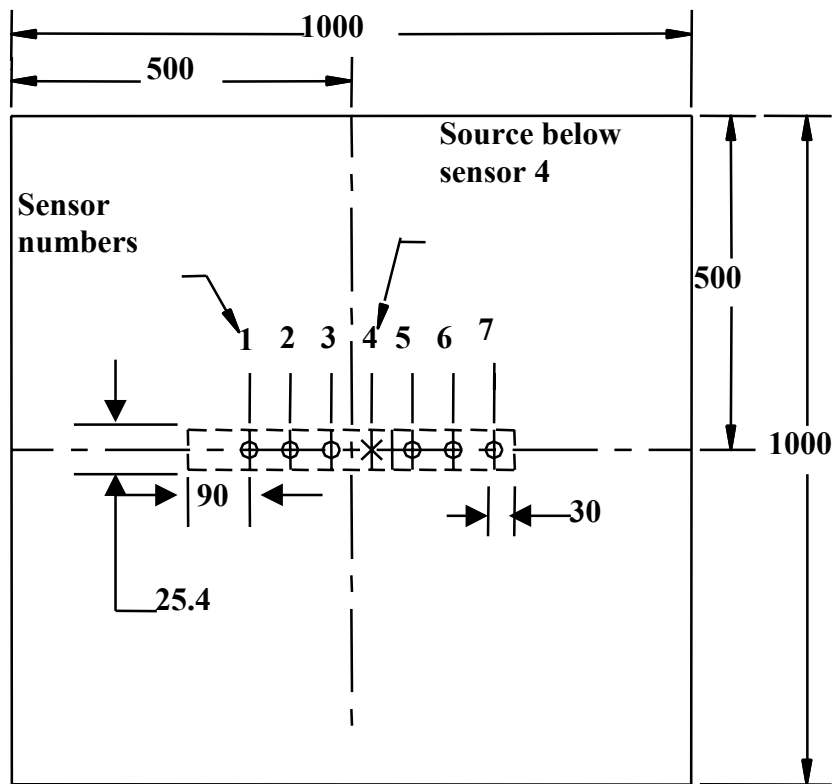


Fig. 1 Finite-element specimens. Dashed lines show the small sample superimposed on the large sample. Sensor numbers show location of sensors, and the source is below sensor 4. All dimensions in millimeters with sensors 60 mm apart.

4. FEM RESULTS AND DISCUSSION

The FEM signals include frequency content from zero hertz up to the highest frequencies generated by the source (based on calculated spectra, a little above the reciprocal of the rise time, hence about 700 kHz to 1 MHz in the current FEM modeling). To more closely approximate signals acquired with real AE sensors, the FEM signals were filtered with a recursive four-pole Butterworth filter. The selected filter ranges were: a bandpass of 100 to 300 kHz for the large

aperture sensor to represent conventional resonant-sensor AE technology, and 40-kHz high-pass for the point-type sensors to represent wideband nearly flat with frequency waveform-based AE technology. In some cases, the point-type sensor signals were also filtered with the 100-to-300-kHz filter.

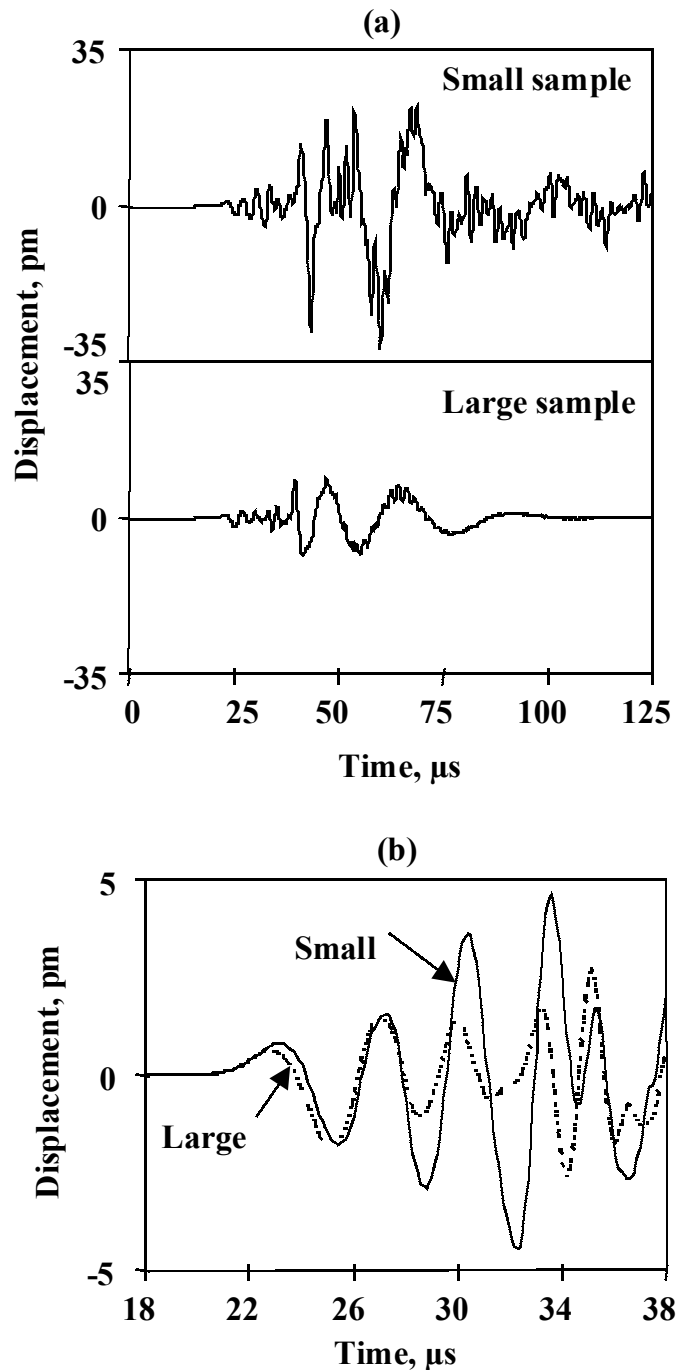


Fig. 2. Comparison of out-of-plane displacement signals at sensor 2 located at 120 mm from the in-plane dipole source centered at a depth of 0.783 mm below the top surface of the plate. (a) a view of longer duration. (b) a view of expanded scale of the early part of the signals from the point-type sensors.

A. Signal Amplitude

Figure 2 compares the FEM-generated signals at sensor 2 for the large and small plate samples. These signals at 120 mm from the source were modeled for the point-type sensor with a single in-plane dipole source (dipole aligned along the axis of propagation to the sensor) with its center located at 0.783 mm below the plate top surface. Figure 2(a) shows the signals with the same vertical displacement scale, and Fig. 2(b) shows the initial portion of both signals with an expanded displacement scale. To provide results with a more complex source, Fig. 3 displays similar views for a microcrack initiation source (three dipoles, major dipole directed along the line of sensors) located at 1.723 mm below the top surface of the plate. These two figures demonstrate the fact that the signals in the laboratory sample have amplitude significantly larger than those in the large sample without nearby edges. The actual peak amplitude increases are about 11.1 dB for the single dipole and about 12.1 dB for the microcrack stimulation. Further, as Figs. 2(b) and 3(b) demonstrate, edge-reflection-based interference and distortion of the signal in the small sample begins only a few microseconds after the direct arrival of the signal. A more extensive examination of the signal database as a function of varying sources, depths and propagation distances indicates that the increase in amplitude of the peak signal relative to the peak amplitude without edge reflections is typically greater at sensors further from the source. As summarized in Table 1, this is consistent for both point-contact sensor signals and finite-aperture sensor signals, and also for both the bandpass of 100 to 300 kHz and the 40-kHz high-pass frequency range. Table 1 also indicates that peak amplitude increases with the point-type sensor were not as large when a bandpass filter of 100 to 300 kHz was used.

Table 1 Observed decibel ranges of increase in peak signal amplitude in the small specimen for the range of source types and depths

	<u>At 60 mm</u> (dB)	<u>At 120mm</u> (dB)
(i) Point-type sensor		
40 kHz H. P. filter	7.4 to 8	9.5 to 10.9
100-300 kHz filter	4.3 to 5.0	6.5 to 7.8
(ii) 13-mm aperture sensor,		
100-300 kHz filter	3.8 to 7.7	6.0 to 9.9

Edge reflections that can superimpose on the direct signals can come not only from the side edges of the small coupon, but also from the ends of the sample. Figure 4 demonstrates this aspect. In this figure, the signals are shown for the point-type sensors with a bandpass of 100 to 300 kHz, located at 60, 120, and 180 mm from the source. The source was an in-plane dipole located at a depth of 0.47 mm below the top surface. The end-edge reflections at the 60-mm and 120-mm sensors are clearly distinguishable from the earlier-arriving part of the signal that is composed of the direct signal and the side-edge reflections. The presence of end-edge reflections modifies the signal propagating from the other direction in a different fashion, as the sensor is positioned more closely to the specimen's edge. In such cases, the part of the end reflection of largest amplitude and the major amplitude portion of the signal coming from the other direction interfere with each other. In such cases, the amplification of amplitude may be further enhanced. We note that these sensor positions were not used in the original referenced experimental study. Also the fact that at the sensor positions of 60 and 120 mm the major-amplitude part of the end-edge reflections are more distinct from the major-amplitude part of the

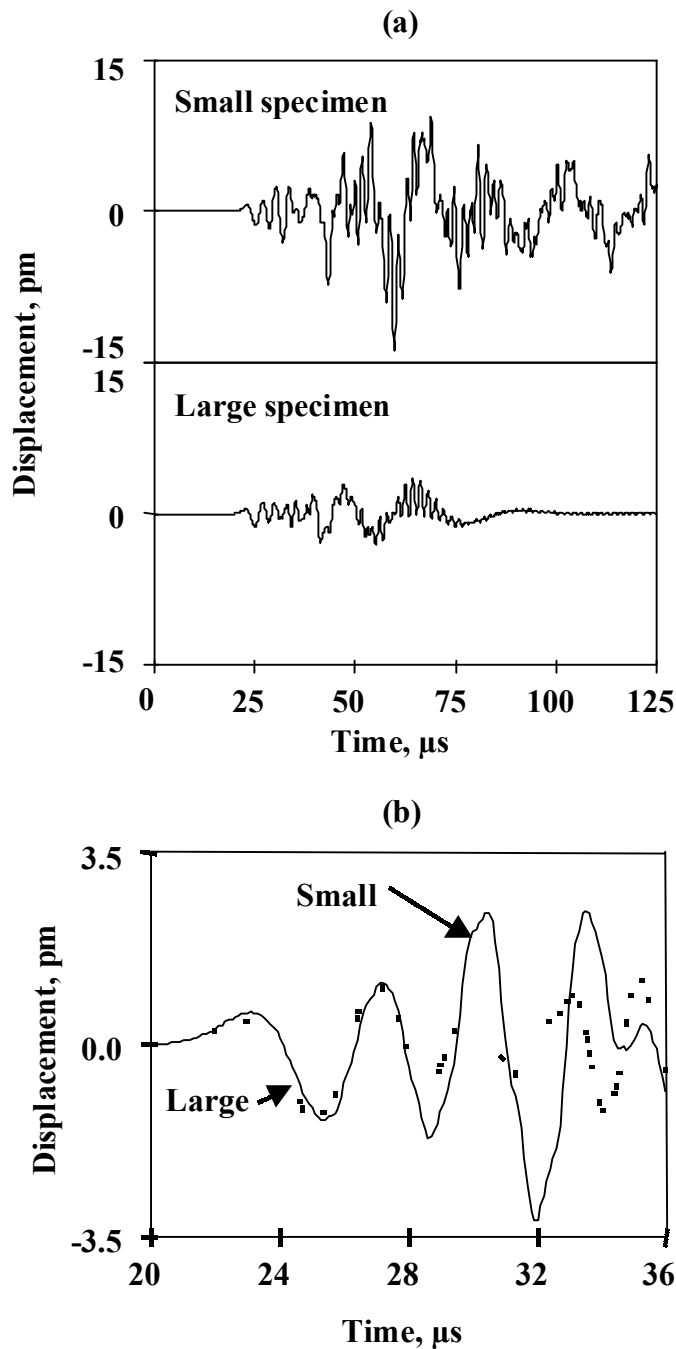


Fig. 3. Same views as in Fig. 2, but for a microcrack initiation source centered 1.723 mm below the top surface of the plate.

signal from the other direction means that these reflections could easily be mistaken as coming from a different AE source event.

Although attenuation due to material-based absorption of the wave is not included in these model calculations, significant decreases in signal amplitudes are observed with increasing propagation distance where no edge reflections are present. The origins of these attenuation effects are both geometric spreading and signal dispersion. This decrease in peak amplitude for the modeled signals versus propagation distance in the large plate is shown in Fig. 5. This figure

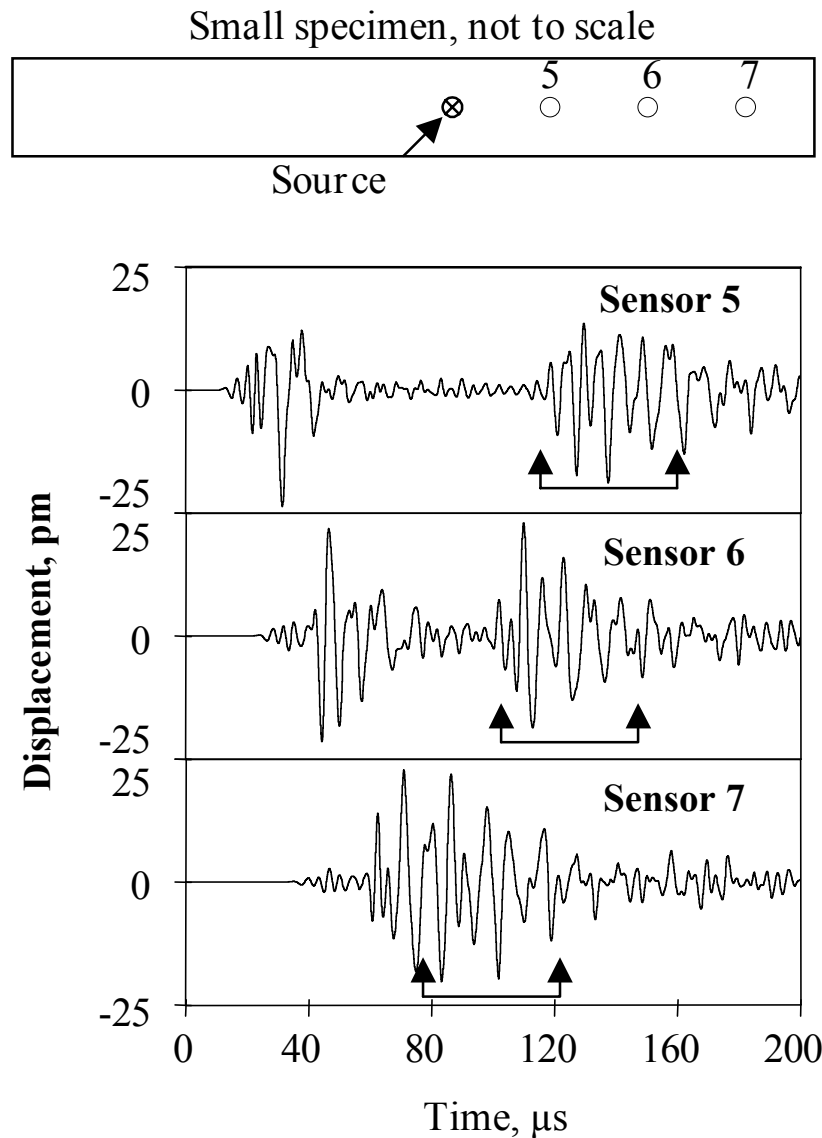


Fig. 4. Out-of-plane displacements at point-type sensors with 100 to 300 kHz bandpass located at 60, 120, and 180 mm from the in-plane dipole source located 0.47 mm below the top surface of the small sample. End-edge reflections from specimen right end shown by connected arrows.

also shows the theoretical prediction for geometric spreading ($1/\sqrt{r}$, where r is the propagation distance from the source). The source for the modeled signals in Fig. 5 was an in-plane dipole located at the mid-plane in the aluminum plate 4.7-mm thick. Additional sensor positions were added for the computation of the data for Fig. 5. The data shown are for the out-of-plane displacement after a 40 kHz high-pass filter for the point-type sensors. It seems clear that the $1/\sqrt{r}$ curve is valid out to 20 mm, but at farther distances dispersion begins to dominate.

In the case of the small coupon sample, the signal attenuation from the two effects of geometric spreading and dispersion is typically partially overcome by the signal amplification from edge reflections. Due to these reflections, a much larger share of the 360-degree radiation of source energy reaches the sensors. We have not calculated any coupon cases where destructive interference between the direct signal and the reflected signals resulted in a decrease

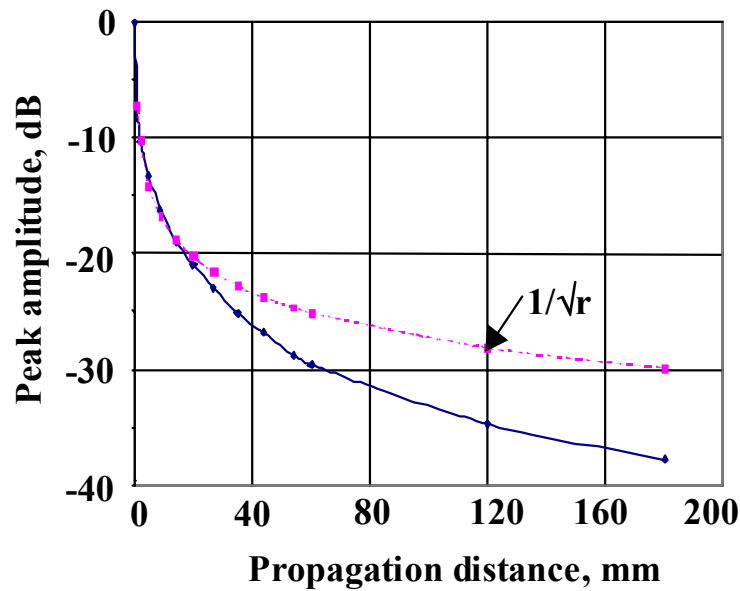


Fig. 5. Calculated loss of AE signal peak amplitude of out-of-plane displacement for a point-type sensor for a mid-plane dipole source with an in-plane orientation. The signal from the large specimen was filtered with a 40 kHz high-pass filter.

in peak signal amplitude. This fact is consistent with the many different reflections that transfer a larger fraction of the original source energy to the sensor in the small coupon. The largest increases in signal (see Table 1) were observed in the case of the 40-kHz high-pass signals with the point-type sensor. One possible explanation for this observation is that a larger fraction of the reflected signals contribute with the point sensor since a wider frequency window allows more of the modes in the reflected signals to contribute to the displacement at the sensor. Also, from Table 1 it is clear that the increases in signal varied considerably as the type and depth of source changed. Further, this table indicates a wider range of signal increases for the large-aperture sensor. This result is likely due to the wider range of reflection paths that can create displacements under the sensor of 13-mm diameter.

The question arises as to whether the observed amount of signal increase is particularly large due to (a) the symmetry of the source, and (b) the sensors being exactly one-half way across the small sample. To examine this question, some finite-element calculations were made with the in-plane dipole source at two non-symmetrical positions. These positions, at 6.13 mm and 3.3 mm from the sample side, are shown in Fig. 6 along with the symmetric position at 12.7 mm from the sample side. Figure 6 also compares the signals for both the symmetric source position and the two different non-symmetric positions. These results were for the point sensor at two distances (60 mm and 180 mm) from the source. Additionally, Fig. 6 includes values of the increase in peak amplitude relative to the same large-sample case. The in-plane dipole source for these calculations was 2.035 mm below the top surface, and the signal was filtered with a 40-kHz high-pass filter. The results shown in this figure indicate that the increases in signal amplitude, while still significant, typically are not as large for the non-symmetric source positions. Table 2 summarizes these results along with similar results for the large-aperture sensors. The range of increases for the large-aperture sensors is typically smaller compared to the point-type sensors.

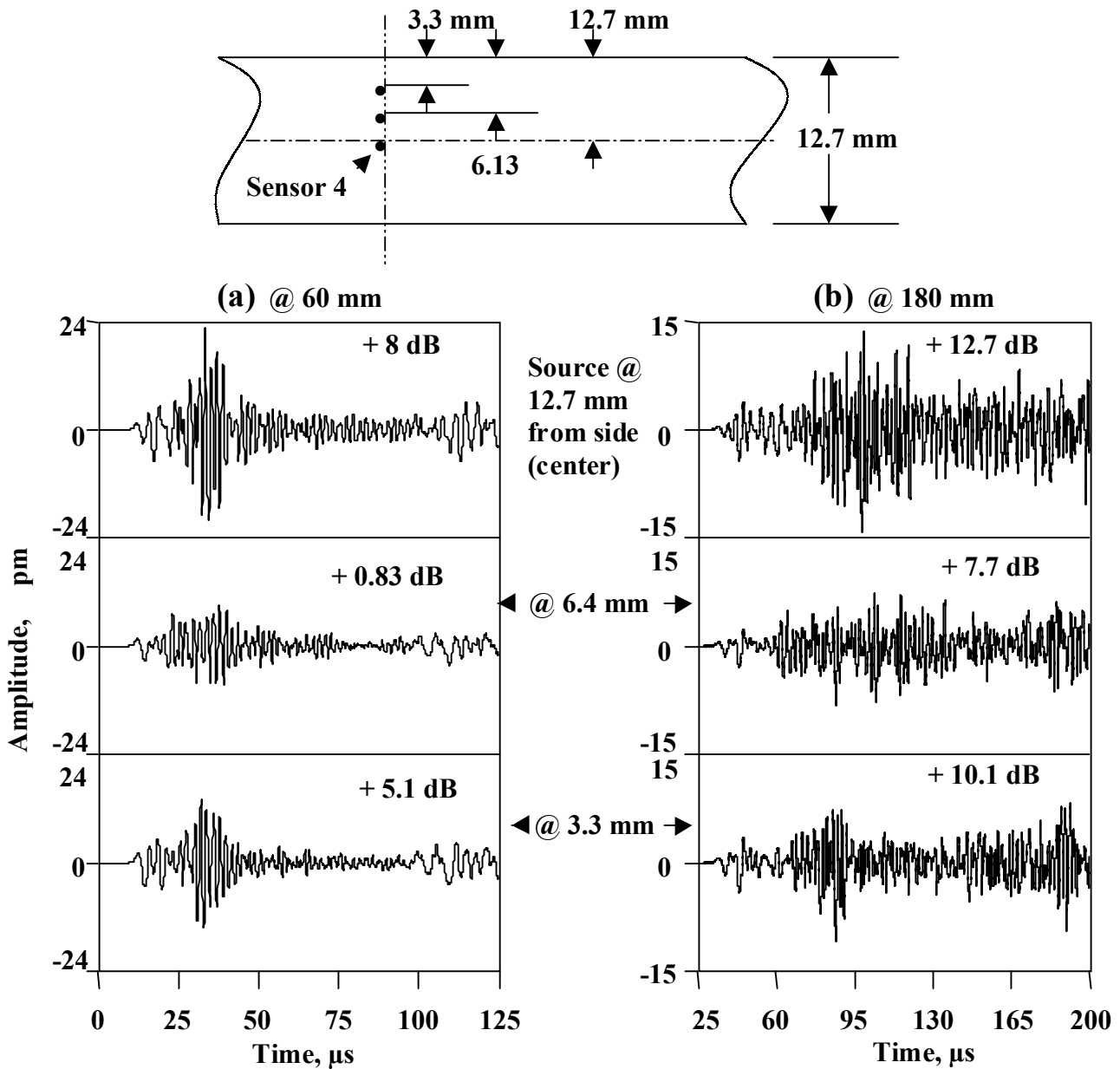


Fig. 6. Examples of point sensor out-of-plane displacement (40-kHz high-pass filter) when the source is located at three different transverse positions (12.7, 6.13, and 3.3 mm from small sample edge as shown, not to scale) in the source plane. Results shown for sensors nominally at 60 mm (sensor 3) and 180 mm (sensor 1) from the source plane with the source centered 2.035 mm below the plate's top surface (at the mid-plane).

The wide range of values as a function of source position and sensor position again results from the many differences in the reflections as these two variables change.

The effects of reflections have some practical implications for both AE field tests and AE laboratory tests. Probably most important is the fact that some AE sources detected in small laboratory coupons will *not* be detected in large specimens. Without the signal amplification from edge reflections, some sources will be hidden by the background noise (electronic noise from the preamplifier) in large samples. Thus, even with the sensors at the same distances

Table 2 Increase (dB) in peak signal amplitude as a function of position of source relative to the small specimen edge

	Symmetric		
	<u>at 12.7 mm</u>	<u>at 6.13 mm</u>	<u>at 3.31 mm</u>
(i) Point-type sensor (40-kHz H.P. filter)			
(a) At 60 mm	8	0.83	5.1
(b) At 120 mm	12.7	7.7	10.1
(ii) Large-aperture sensor (100-300 kHz)			
(a) At 60 mm	9	0.1	3.8
(b) At 120 mm	10.3	1.5	4

relative to the source as in a small laboratory coupon, the database of detected signals will be smaller for large samples (same material and thickness) than for a coupon. A second important aspect relates to the use of peak amplitudes for source identification in a laboratory-size sample. As Fig. 6 shows, moving the sensor from 60 to 180 mm from the source typically results in a loss of signal amplitude (note vertical scale goes from ± 24 pm to ± 15 pm). An even larger effect is the potential change in peak amplitude as the source is moved laterally across a single cross-sectional source plane (from Fig. 6, 0.83 to 8 dB at 60 mm and 7.7 to 12.7 dB at 180 mm). In addition to the dependence of peak amplitude on lateral source positions, the peak amplitude also changes with the depth of the source. Figure 7 demonstrates these changes in the small specimen at 120 mm from the source. The point-type sensor results (40 kHz high pass at sensor 2) shown in this figure are for an in-plane dipole at depths of 0.47 mm and 2.35 mm (mid-plane). The peak amplitude difference for the same source at these two different depths is about 9.3 dB. The equivalent large-aperture sensor data (100 to 300 kHz bandpass) produces a difference of about a 8.1 dB in the small specimen. For the large sample, the peak amplitude changed by about 8.9 dB with the point sensor, and by about 8.4 dB for the large-aperture sensor under the same conditions.

B. Spectra of Signals

Numerous users of AE have attempted to use the frequency spectrum of an AE signal for the purpose of source identification. The premise for such studies is that different source types will have different frequency spectra. We note that some researchers have recognized the need to use wideband sensors of small aperture and relatively flat with frequency response, in such experiments. Typically, experiments analyzing frequency spectra have been performed in the laboratory with relatively small samples, which inherently have nearby edges. In some cases, the AE researchers have recognized that edge reflections could cause a problem. This recognition leads to the technique of calculating the spectrum of only some arbitrarily selected early portion of the measured signal. The database developed by the FEM modeling provides for a systematic investigation of the effects on spectra of reflections from nearby specimen edges in coupon specimens.

To develop key insight into the effects of edge reflections on spectra, we will first examine some results obtained from FEM calculations with the large sample. Figure 8 shows the out-of-plane displacement (40 kHz high-pass) for point sensors located at 180 and 60 mm from an in-plane dipole located at the mid-plane. The reflection from the left edge of the sample is shown by an arrow for both propagation distances. These reflections follow the expected pattern of

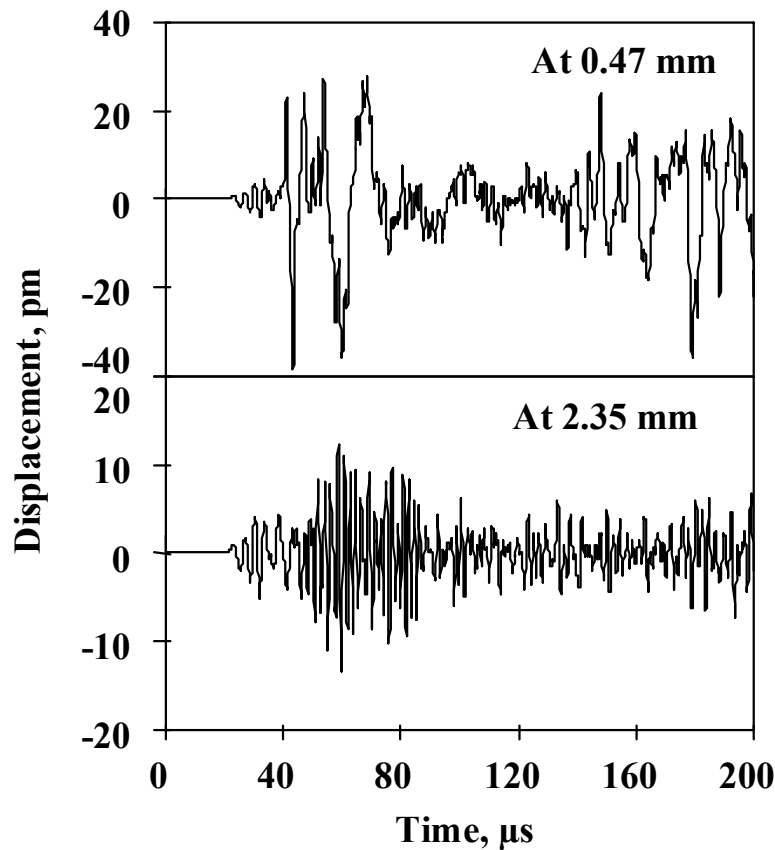


Fig. 7. Out-of-plane displacement in small sample at 120 mm for the same in-plane dipole source located at two different depths (0.47 mm and 2.35 mm below the top surface).

arriving first at the sensor farthest from the source, since it is nearer the left edge of the large sample. If the whole signal shown in Fig. 8(a) is used to calculate the Fast Fourier Transform (FFT), the result is shown in Fig. 9(a). If the signal in Fig. 8(a) is truncated at 145 μs (i.e. before the reflection arrival) and the FFT is calculated the result is shown in Fig. 9(b). As a part of the FFT calculation, both signals were extended with zeros so as to have the same number of points. By comparing Figs. 9(a) and 9(b) it is clear that the spectrum shown in Fig. 9(a) has been distorted due to the presence of the small reflected signal. Further, the distorted region of the frequency spectrum is the frequency range contained in the reflection signal. This fact was verified by calculating the FFT of the reflection signal and showing that it was nearly identical to the FFT of the first part of the direct signal. If we examine the spectrum for the same source case (0 to 145 μs signal) but in the small specimen, the presence of substantial distortion is shown in Fig. 10(a). Notice also that the peak amplitude of the spectrum in the small specimen is more than 16 dB higher than that in the large sample (Fig. 9(b)).

It is interesting to note that, if the result in Fig. 10(a) is substantially smoothed, then as shown in Fig. 10(b) a spectrum more similar to that of the large specimen (Fig. 9(b)) can be obtained. The amount of smoothing necessary was determined by trial and error. If Fig. 9(b) had not been available then the appropriate smoothing (in this case, over 150 kHz portions or over 30 digital points) could not have been easily determined.

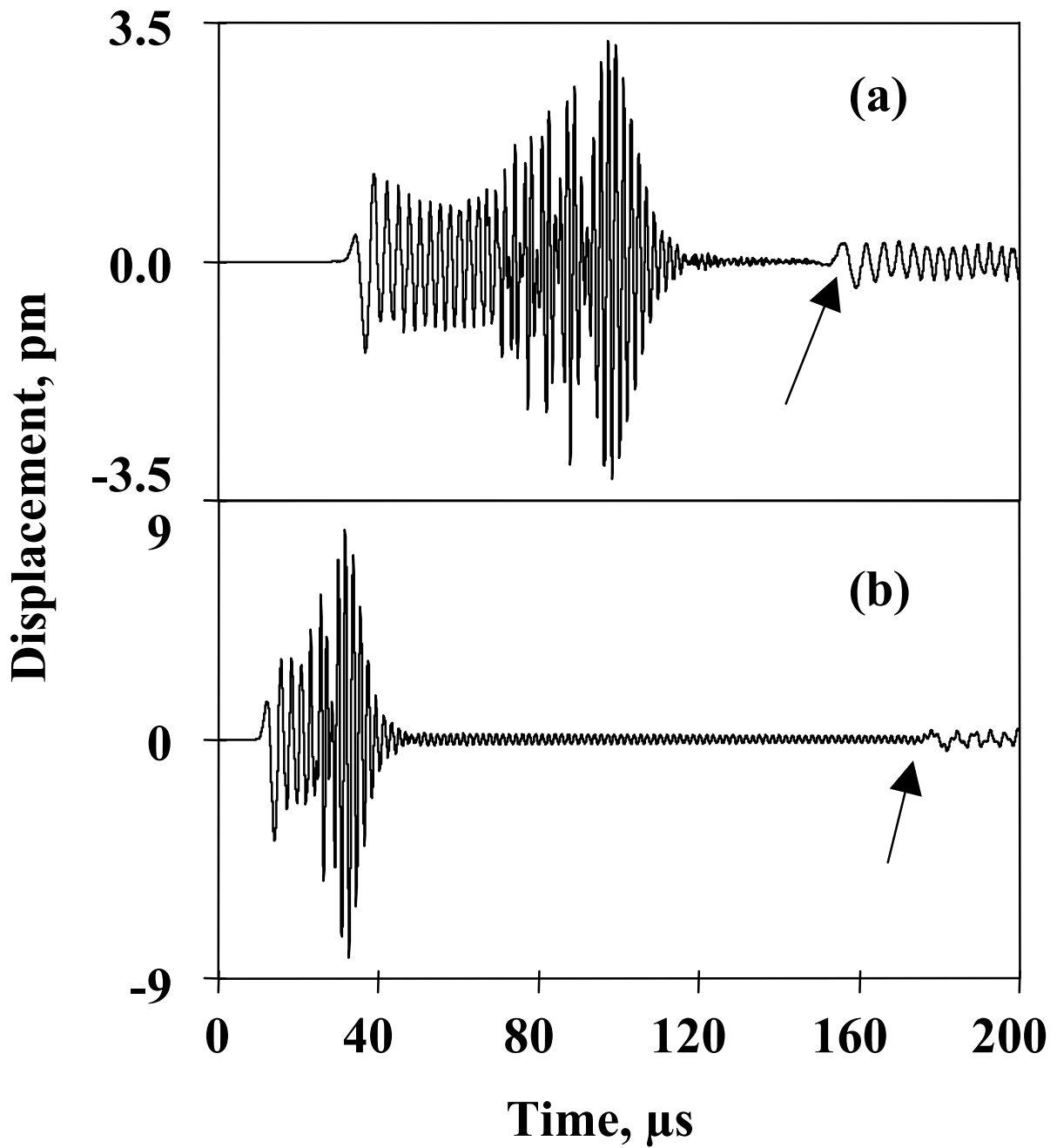


Fig. 8. Out-of-plane displacement (with point sensors and 40-kHz high-pass filter) at (a) 180 mm and (b) 60 mm from the source in the large sample. Edge reflection indicated by arrows. Source is an in-plane dipole located at the mid-plane.

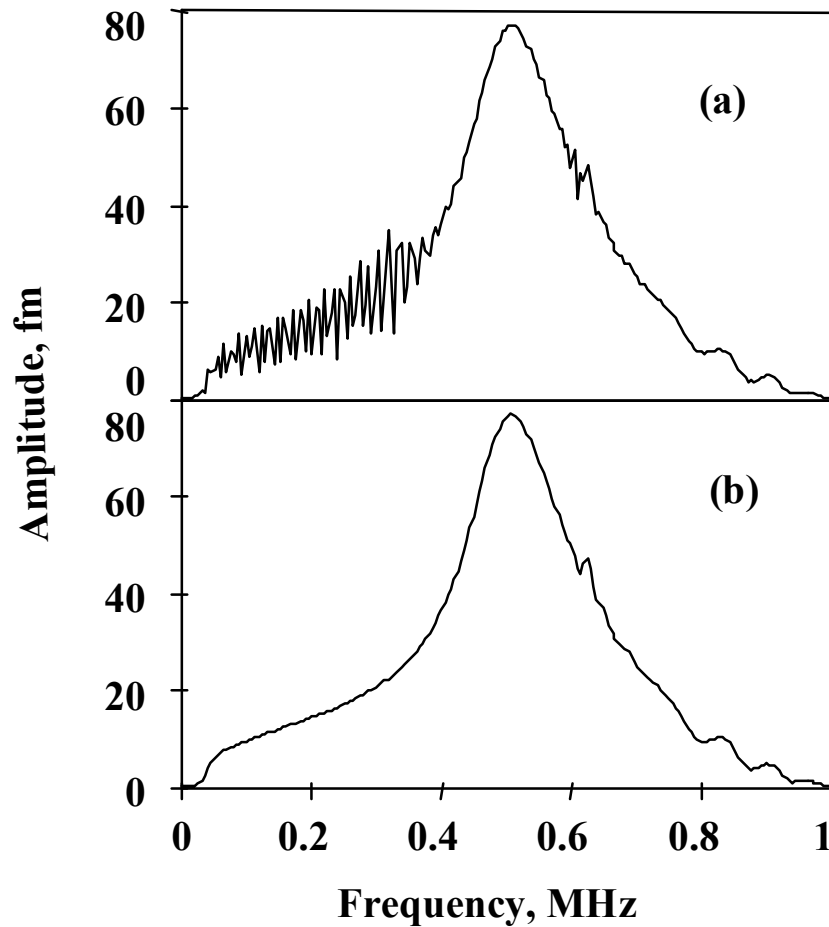


Fig. 9. FFT spectra of the signal shown in Fig. 8(a). Fig. 9(a) is for the whole time domain out to 200 μs (including the edge reflection of the highest-velocity part of the fundamental symmetric mode), and Fig. 9(b) is for the same time-domain signal truncated at 145 μs (prior to the reflection).

Distortion of the AE signals and their FFT due to edge reflections has several implications for the materials researcher who is attempting to use AE techniques to identify different damage mechanisms. Most obvious is that the use of a large sample that does not result in early edge reflections would significantly enhance the determination of the basic source characteristics of AE signals as determined in the far-field. This size sample has been used to monitor growth of fatigue cracks (Hamstad and McColskey, 1999). Further, the approach of using only a small portion of the beginning of the AE signal to calculate the FFT in small specimens does not provide useful information for identification of AE sources. The reason for this is two-fold. First, truncating the time-domain signal may eliminate source information present in the slower-velocity (direct-path) components of the signal. Second, even the early-arriving parts of the signal have experienced distortions from early edge reflections. These effects are illustrated in Fig. 11. Starting from the top of Fig. 11(a), a series of five truncated signals is shown for a small specimen with an in-plane dipole source located at 1.723 mm below the top surface. The point-type sensor data (40 kHz high-pass) are for a sensor located at 60 mm from the source epicenter. The durations of the *non-zero* portion of the signals are 10, 20, 30, 110, and 165 μs . The bottom signal in this figure is the large-specimen equivalent case truncated at 175 μs total duration.

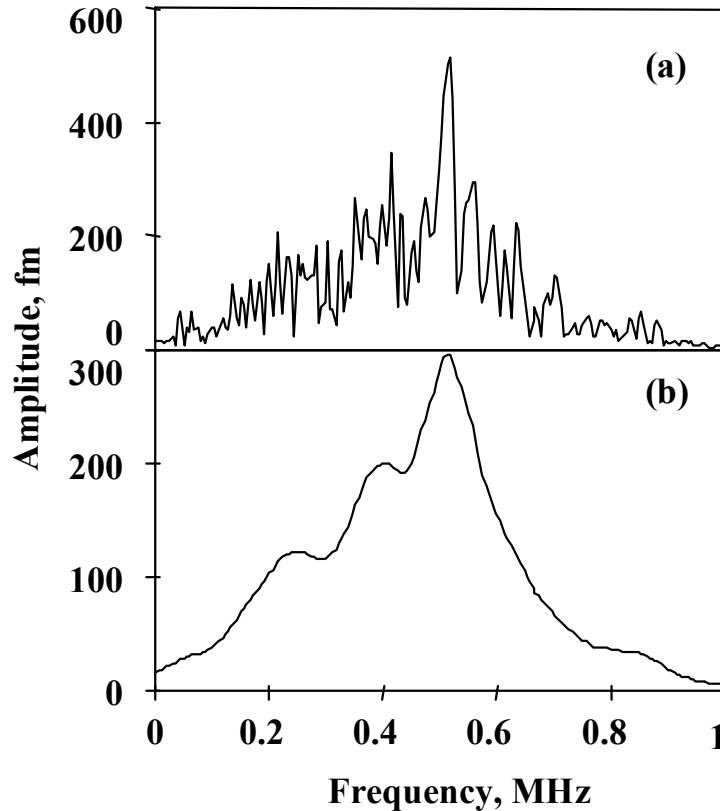


Fig. 10. FFT spectra of a 145- μ s portion of the out-of-plane displacement at 180 mm for an in-plane dipole source located at the mid-plane of a small sample. (a): the spectrum without smoothing; (b): a smoothed version of (a). Note that the source type and location (relative to the sensor) is the same as shown in Fig. 9 for the large sample.

Figure 11(b) shows in the same order the calculated FFTs of the signals. We note that prior to calculating the FFTs all the signals were extended with zeros to the same number of points. Clearly the FFTs of the early part of the signal in the small sample fail to include the essence of the real spectrum as shown at the bottom of Fig. 11(b). And in fact a *longer* truncated signal (e.g. 110 μ s of non-zero signal) provides a more correct (but still distorted) result. The reason for this fact, as indicated above, is that the slower-velocity parts of the signal define significant aspects of the true signal FFT. We conclude that it is not surprising that AE source identification by the use of spectra has not been a broadly successful approach since most researchers attempting to do this have used small samples.

C. Concluding Remarks

The user of AE technology who does not understand the effects of nearby specimen edges can make incorrect conclusions. On one hand, a field practitioner testing a large sample without nearby edges may not detect damage-indicating AE events. These same events may have been easily detected in small laboratory coupons due to edge reflections that amplify the direct signal. Further, if events are detected in the field case, the field practitioner may underestimate their significance. The reason is that the events will not have the amplitude, energy and duration levels associated with the same original source amplitude in the results for laboratory coupons. On the other hand, the materials scientist attempting to use AE techniques to identify certain

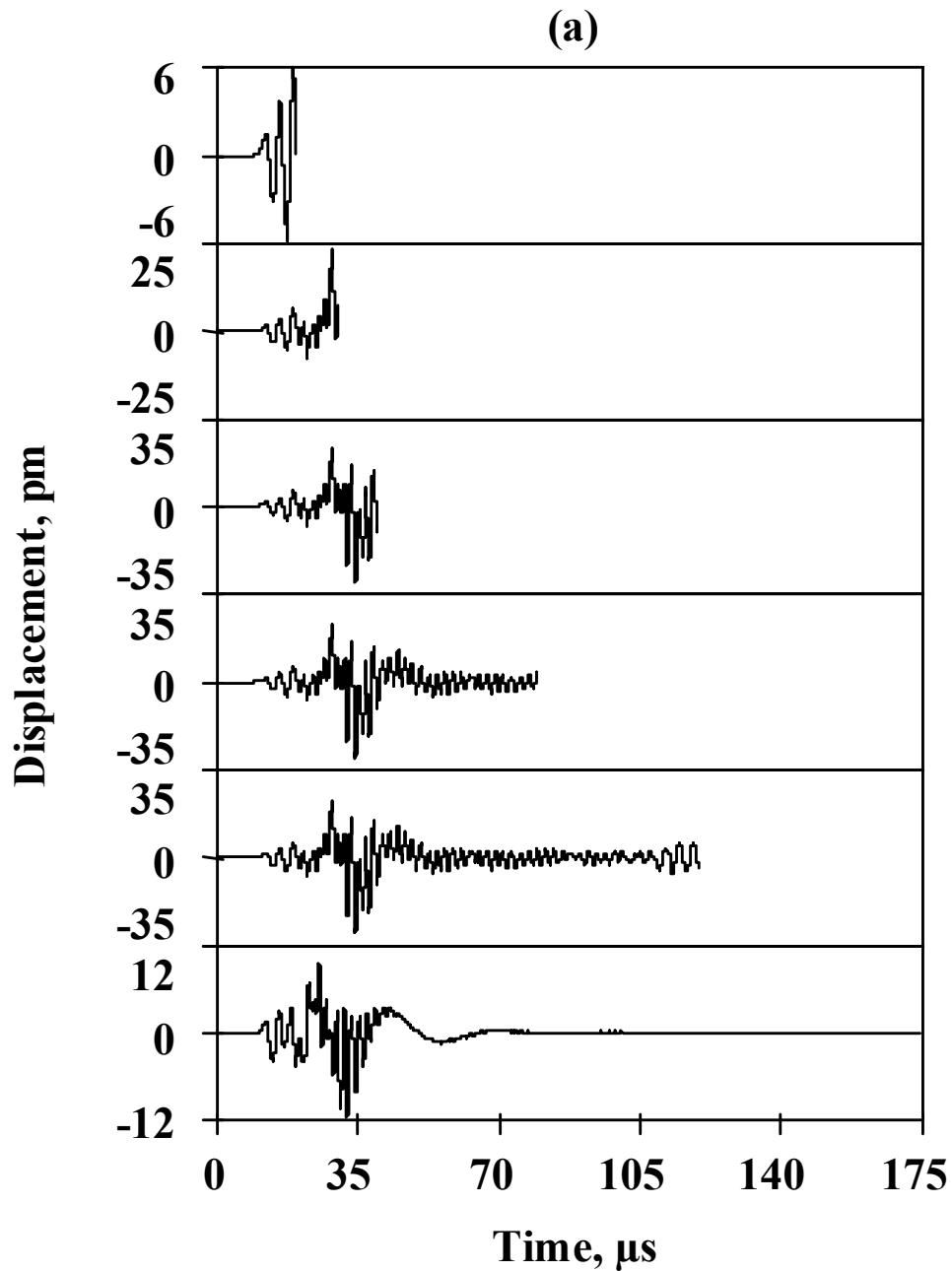


Fig. 11. (a) Out-of-plane displacement signals (truncated at different lengths) at 60 mm from the source.

types of damage in a small laboratory coupon may become frustrated with the lack of consistency in source identification using features such as the hit peak amplitude, energy, duration, and frequency content. In addition, the materials scientist may find that the distorted frequency spectra make it difficult or impossible to distinguish one type of source from another. Finally, we believe the development of AE technology could experience a much larger payoff in the practical application of the technology to large samples if associated laboratory research were regularly carried out on larger samples.

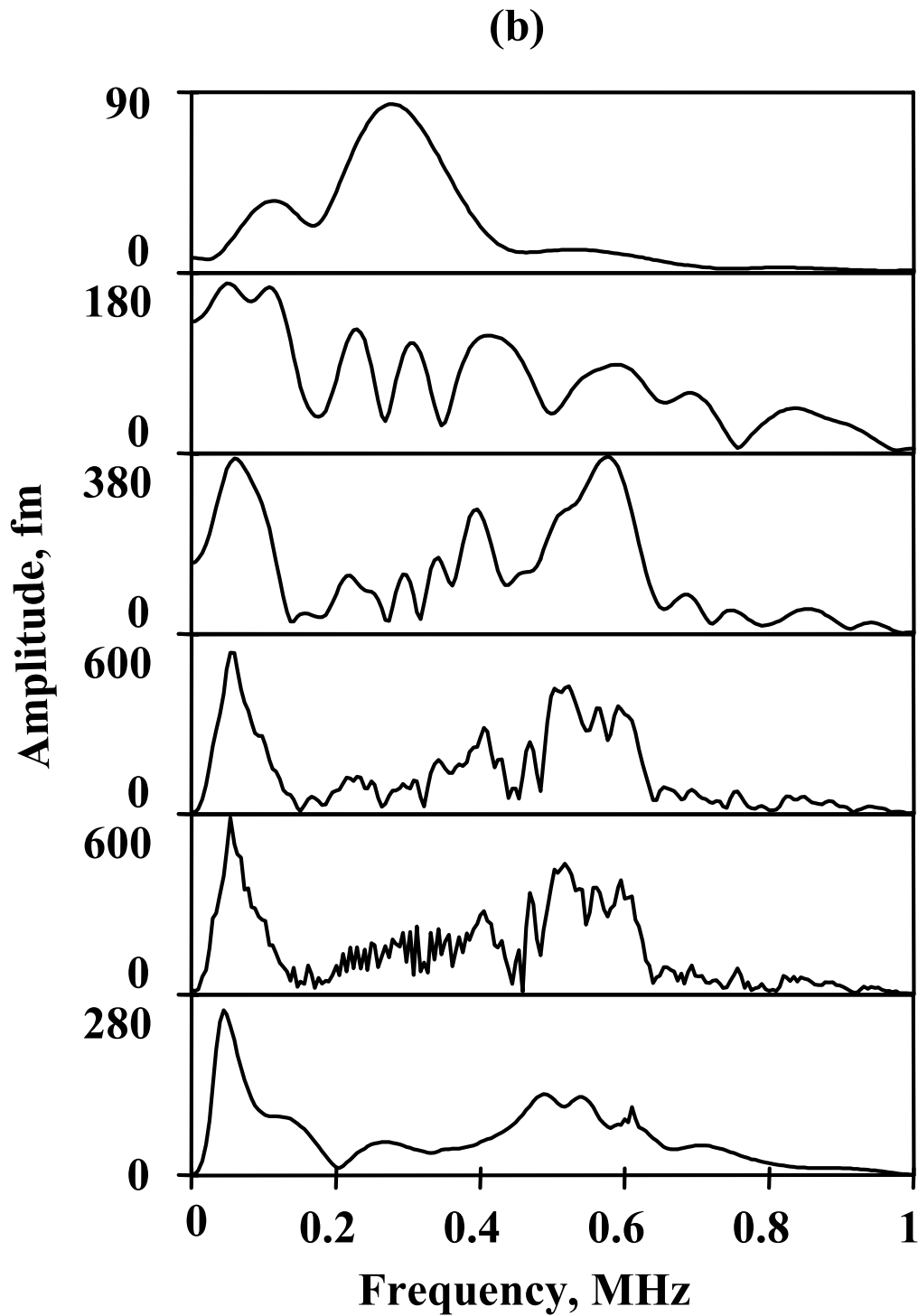


Fig. 11(b): FFTs for the signals in Fig. 11(a). In each figure, the first five plots (starting from the top) are for a small specimen, and the bottom plot is for the equivalent large specimen. The source was an in-plane dipole located at 1.723 mm below the plate's top surface in the small and large specimens, and the signals were for a point-type sensor (40-kHz high-pass).

REFERENCES

- M. R. Gorman (1998), "Some connections between AE testing of large structures and small samples," *Nondestr. Test. Eval.*, **14**, 89-104.
- M. A. Hamstad, A. O'Gallagher, and J. Gary (1999), "Modeling of buried monopole and dipole sources of acoustic emission with a finite element technique," *J. Acoust. Emission*, **17**(3/4), 97-110.
- M. A. Hamstad and J. D. McColskey (1999), "Detectability of slow crack growth in bridge steels by acoustic emission," *Materials Evaluation*, **57**(11), 1165-1174.
- S. L. McBride and Y. Hong (1992), "Acoustic emission from crack growth in 7050 aluminum and 7075 aluminum as a function of temperature and heat treatment," *Progress in Acoustic Emission VI*, edited by T. Kishi, K. Takahashi, and M. Ohtsu, The Japanese Society for NDI, Tokyo, pp. 521-528.
- W. H. Prosser, M. A. Hamstad, J. Gary, and A. O'Gallagher (1999), "Reflections of AE waves in finite plates: finite element modeling and experimental measurements," *J. Acoust. Emission*, **17**(1/2), 37-47.
- C.B. Scruby (1985), "Quantitative acoustic emission techniques," Chapter 4 in *Non-destructive Testing, Vol. 8*, Academic Press Inc., London, pp. 141-210.